Mixing in fully chaotic flows

A. Wonhas

*Department of Applied Mathematics and Theoretical Physics, University of Cambridge, Silver Street,
Cambridge CB3 9EW, United Kingdom*

J. C. Vassilicos

Department of Aeronautics, Imperial College, London SW7 2BY, United Kingdom

Passive scalar mixing in fully chaotic flows is usually explained in terms of Lyapunov exponents, i.e., rates of particle pair separations. We present a unified review of this approach (which encapsulates also other nonchaotic flows) and investigate its limitations. During the final stage of mixing, when the scalar variance decays exponentially, Lyapunov exponents can fail to describe the mixing process. The failure occurs when another mixing mechanism, first introduced by Fereday *et al.* [Phys. Rev. E **65**, 035301 (2002)], leads to a slower decay than the mechanism based on Lyapunov exponents. Here we show that this mechanism is governed by the large-scale nonuniformities of the flow which are different from the small scale stretching properties of the flow that are captured by the Lyapunov exponents. However, during the initial stage of mixing, i.e., the stage when most of the scalar variance decays, Lyapunov exponents describe well the mixing process. We develop our theory for the incompressible and diffusive baker map, a simple example of a chaotic flow. Nevertheless, our results should be applicable to all chaotic flows.

I. INTRODUCTION

The mixing of a diffusive passive scalar quantity Θ advected by a fluid flow can be characterized by the decay properties of the scalar field's variance $E \equiv \int d\mathbf{x}\,\Theta^2 - (\int d\mathbf{x}\,\Theta)^2$ when no source of scalar is used to replenish the variance lost through mixing (no scalar forcing). In fully chaotic incompressible flows, where the term "fully" refers to the absence of Kolmogorov-Arnold-Moser surfaces [1], effectively all trajectories are chaotic and no regions exist where trajectories are integrable. Such flows exhibit an exponential scalar variance decay in the long time limit [2–5]. Pierrehumbert [2] also conjectured that the decay rate becomes independent of molecular scalar diffusivity in the limit of very small diffusivities. Antonsen, Fan, Ott, and Garcia-Lopez [5] (in the following AFOG96) have identified and explained one mechanism that generates such an exponential long-time variance decay (see also Ref. [6]). In this introduction, it is motivating to summarize and generalize their train of thought, which even though heuristic is, nevertheless, instructive. In the main part of this paper we identify, in turn, a long-time variance decay mechanism that is conceptually different from AFOG96 and shows the limitations of their argument.

Separation of particle pairs. Incompressible two-dimensional flows are such that, at any point and any time, there is a direction along which velocity gradients cause particle[1] pairs to separate faster than in any other direction, and another direction along which particle pairs either contract (as in straining flows) or simply do not separate nor contract at all (as in shearing flows). We make this well-known statement in the context of two-dimensional flows for

convenience of exposition, but also because AFOG96 have limited their own exposition to two-dimensional flows. However, nothing prevents us, in principle, from extending this statement and the following heuristic argumentation to incompressible three-dimensional flows.

Particle pair separations and scalar field gradients. AFOG96 effectively consider, on the one hand, the localized gradients of a scalar field $\Theta(\mathbf{x},t)$, and on the other hand vectors connecting the individual particles of particle pairs (particle pair vectors). A flow can accelerate the decay of the scalar field variance by causing the scalar field gradients to grow. In the long-time limit, after the gradients have orientated themselves orthogonal to the direction of fastest growing particle separation, incompressibility implies that the inverse length scale defined by the local scalar gradient, i.e., $|(1/\Theta)\nabla\Theta|$ has the same time dependence as the locally fastest growing particle pair separation. We denote this fastest growing separation by $\Delta_+(\mathbf{x},t)$ and note that it potentially has different growth rates in different positions $\mathbf{x}$. In straining or chaotic flows, where the particle pair separation Δ_+ grows on average exponentially with time, the proportionality constant of gradient growth depends like $|(1/\Theta)\nabla\Theta| \propto \sin\phi\,\Delta_+$ on the initial angle $\phi \neq 0, \pi$ between the local gradient and the direction of the locally fastest growing particle separation [see Eqs. (13)–(17) in AFOG96]. In shearing or vortical flows, however, where the particle pair separation Δ_+ grows on average linearly with time, the initial condition is forgotten for long enough times and hence the growth rate does not depend on the initial angle $\phi \neq \pm \pi/2$. Dimensional considerations force us to write

$$\left|\frac{1}{\Theta}\nabla\Theta\right| \propto s(\phi)\frac{\Delta_+}{a_0}, \tag{1}$$

where a_0 is some conserved characteristic area. The func-

---

[1] In this paper "particle" is used to mean "fluid element."

tions $s(\phi)$ and a_0 express the dependence on initial conditions for different types of flow. For straining or chaotic flows $s(\phi) = \sin(\phi)$, and for shearing or vortical flows $s(\phi)$ is constant. The particle separation also behaves differently in different types of flow. AFOG96 only consider the case of fully chaotic flows where h is a Lyapunov exponent and $\Delta_+ = \Delta_0 e^{ht}$ for sufficiently long times. However, it is very instructive not to limit ourselves to chaotic flows at this stage and see how far we can go without specifying a particular type of particle separation.

Gradients and variance decay. From the advection-diffusion equation $(D/Dt)\Theta = \kappa \nabla^2 \Theta$, where (D/Dt) is the material (or hydrodynamic) derivative and κ is the molecular diffusivity of the scalar Θ, we deduce that

$$\frac{D}{Dt}\frac{1}{2}\Theta^2 = -\kappa|\nabla\Theta|^2 + \kappa\nabla\cdot(\Theta\nabla\Theta), \qquad (2)$$

which leads to

$$\frac{D}{Dt}\Theta^2 = -2\kappa s^2(\phi)\frac{\Delta_+^2}{a_0^2}\Theta^2 + 2\kappa\nabla\cdot(\Theta\nabla\Theta), \qquad (3)$$

where we have absorbed a dimensionless constant of proportionality inside a_0. In the case where the length scale of the flow is much larger than the length scales of scalar fluctuations, it might be assumed that the scalar length scales vary slowly in space and, therefore, that gradients of terms involving gradients of Θ are negligible. On this basis $\nabla\cdot(\Theta\nabla\Theta)$ can be neglected in the last two equations leaving us with

$$\frac{D}{Dt}\Theta^2 \approx -2\kappa s^2(\phi)\frac{\Delta_+^2}{a_0^2}\Theta^2. \qquad (4)$$

A Lagrangian integration along a particle path starting at a point $\mathbf{x}$ gives

$$\Theta^2(\mathbf{x},t) = \Theta_0^2(\mathbf{x})\exp\left[-2\kappa a_0^{-2}s^2(\phi)\int_0^t d\tau\Delta_+^2\right], \qquad (5)$$

where the time integral is along the history of a particle pair, i.e., a particle and the particle pair vector on this particle. Note that both ϕ and Δ_+ are functions of $\mathbf{x}$. Hence, assuming without loss of generality that $\int d\mathbf{x}\,\Theta = 0$, the scalar variance $E(t) \equiv \int d\mathbf{x}\,\Theta^2 - (\int d\mathbf{x}\,\Theta)^2$ takes the form

$$E(t) = E(0)\int d\mathbf{x}\frac{\Theta_0^2(\mathbf{x})}{E(0)}$$

$$\times\exp\left[-2\kappa a_0^{-2}s^2(\phi)\int_0^t d\tau\Delta_+^2(\mathbf{x},\tau)\right]. \qquad (*)$$

Star equation. Let us mark this equation by a star to distinguish it from all other equations in this paper and let us refer to it as the star equation. The reason why this equation attracts our interest is twofold. The first reason is conceptual: this equation directly relates the decay of the scalar variance, which is a measure of mixing, to the growth of particle pair separations, which is a measure of stirring. It implies that a Lagrangian analysis of particle pair histories is enough to determine the rate of decay of the scalar variance. (A conceptually similar yet very different formula in terms of propagators has been given in the context of statistical fluid mechanics by Durbin [7] for the calculation of scalar variance profiles in space and/or their time dependence.) The second reason is that, despite the imperfect nature of its heuristic derivation, the star equation leads to right answers not only in some instances and regimes of two-dimensional incompressible and fully chaotic flows [5] but also when the flow is a two-dimensional incompressible steady or slightly unsteady vortex [8,9].

Variance decay in chaotic flows. In the case of fully chaotic flows, AFOG96 have assumed that the angles ϕ are randomly distributed and independent of Δ_+ and that the integration over space in the star equation can be replaced by an integration over the Lyapunov exponents h and angles ϕ leading to

$$E(t) = E(0)\int dh\mathcal{P}(h,t)\int_0^{2\pi}\frac{d\phi}{2\pi}$$

$$\times\exp\left[-\kappa L^{-2}\sin^2\phi\frac{\exp(2ht)-1}{h}\right], \qquad (6)$$

where $\mathcal{P}(h,t)$ is the probability density function for h, where use has been made of $s(\phi) = \sin\phi$ and $\Delta_+ = \Delta_0 e^{ht}$, i.e., assuming a history with constant strain for each particle pair separation, and finally where L is a characteristic length scale of the initial scalar field such that $a_0 = L\Delta_0$. The point that AFOG96 make, which allows them to identify a mechanism for exponential long-time variance decay, is that in the long-time limit, $[\exp(2ht)-1]/h$ is very large and the dominant contribution to the integral comes from small values of $\sin\phi$. Hence, AFOG96 argue that in the case of fully chaotic flows, the dominant long-time contribution to the decay of scalar variance comes from gradients orientated close to the direction of largest positive Lyapunov exponent ($\phi=0,\pi$) because these gradients are the last ones to survive molecular diffusion. A straightforward expansion around $\phi=0$ and $\phi=\pi$ followed by the ϕ integration does indeed lead to an exponential decay of $E(t)$. AFOG96 go on to estimate $\mathcal{P}(h,t)$ and find quantitative agreement between the exponential long-time decay predicted by their theory and the exponential long-time decay found in a computer simulation of a case of fully chaotic scalar advection and diffusion.

Variance decay in vortical flows. In the case of steady vortical flows, as in the case of any steady shear flow, the particle separations grow linearly for sufficiently long times ($Lht \gg \Delta_0$), i.e., $\Delta_+ \approx Lht$, where the local shear rate h is given by $h = \Omega_0 g(\mathbf{x})$, Ω_0 being the angular velocity of the vortex at a distance L from its center and g is an appropriate dimensionless function of space. Choosing L to be a length scale characterizing the position of the initial scalar patch with respect to the vortex, inserting this type of particle pair separation in the star equation with $a_0 = L^2$ and considering $s(\phi) = $ const, the star equation becomes

$$E(t) = E(0) \int d\mathbf{x} \frac{\Theta_0^2(\mathbf{x})}{E(0)} \exp\left[-\frac{2}{3}\text{Pe}^{-1} g^2(\mathbf{x})(\Omega_0 t)^3 \right],$$

$$(7)$$

where $\text{Pe} \equiv \Omega_0 L^2 \kappa^{-1}$. This equation is effectively the same as Eq. (2.12) in Ref. [8] except that these authors use nondimensionalized space and time variables, polar coordinates for their spatial integration, and an azimuthal Fourier series. One can follow a nearly identical argumentation as that of Ref. [8] between their equations (2.12) and (2.19) to obtain the right decay law

$$E(0) - E(t) \propto (\text{Pe}^{-1}\Omega_0^3 t^3)^{1-D'} \qquad (8)$$

in terms of the Kolmogorov capacity D' (fractal codimension, $D' < 1$) of the spiral gradient structure imposed on the scalar field by the two-dimensional vortex. This algebraic decay law of the scalar variance in a steady two-dimensional vortex is valid in the time range $1 \ll \Omega_0 t \ll \text{Pe}^{1/3}$. It has already been obtained by a direct asymptotic analysis of the advection-diffusion equation without recourse to the star equation and has also been computationally verified [8,9].

Limitations of the star equation. The star equation provides, therefore, good results in two extreme and diametrically opposed cases of incompressible flow: fully chaotic flows and steady vortices. Nevertheless, the extent of applicability of this equation and of the Lagrangian approach that it encapsulates remains unclear. In this paper we show that the star equation can also be applied successfully to the early time behavior of scalar variance decay in fully chaotic flow. However, we identify a mechanism that is conceptually different from the Lagrangian one of AFOG96 and which also leads to long-time exponential variance decay in fully chaotic flow. This mechanism is governed by the contracting directions of negative Lyapunov exponents and is not incorporated in the star equation. In fact, the AFOG96 argument based on the star equation predicts that there is no residual mixing in the contracting directions in the long-time limit. There must therefore be situations in cases of fully chaotic flow and perhaps other flows too, where the Lagrangian approach of the star equation cannot predict the right mixing properties and scalar variance decay. Generally, however, both mechanisms should be expected to coexist. Depending on initial conditions and relative strength, i.e., decay rates, of both mechanisms, one or the other might prevail and determine mixing. We leave this issue for future study and concentrate here specifically on the non-Lagrangian mechanism of scalar variance decay.

Our model. In this paper we focus our attention on the incompressible baker map to which we add molecular diffusion for the study of mixing. This map is a good model of the stretch and fold mechanism that is at the heart of chaotic advection. The entire paper is devoted to the effect of the baker map on a scalar field which is so orientated that only the contracting direction of the map acts on it. This is exactly the situation for which the star equation predicts faster scalar variance decay than exponential in the long-time limit. Nevertheless the model yields exponential long-time behavior.
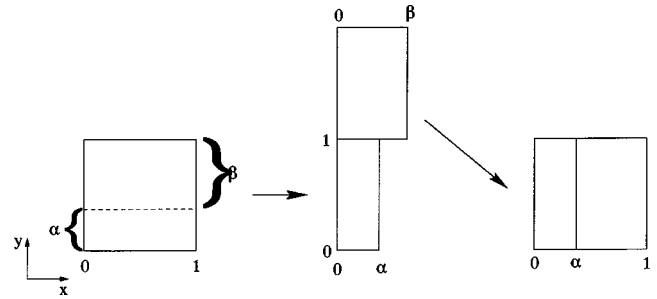
FIG. 1. Illustration of the incompressible baker map. The unit square is divided horizontally at a height α. The resulting lower rectangle is horizontally compressed by the factor α and vertically stretched by $1/\alpha$. Similarly, the upper rectangle is horizontally compressed by β and vertically stretched by $1/\beta$. Finally, the upper rectangle is moved down to the right to join the lower rectangle such that a unit square is regained.

Outline of the paper. The model and its scalar decay properties are given in Sec. II. In Sec. III we successfully apply the star equation to calculate the early time decay of the scalar variance. The vast majority of the variance is in fact lost in these early stages. Following the early time decay, the scalar variance decay is exponential in time and governed by a mechanism first introduced in Ref. [10]. We study this decay mechanism in Secs. IV and V and explain it in terms of large-scale nonuniformities of the map. Issues to do with universality are also addressed in these sections. We conclude in Sec. VI.

II. THE INCOMPRESSIBLE AND DIFFUSIVE BAKER MAP

Advection of baker map. The incompressible baker map [11] is an idealized model for advection by an incompressible fully chaotic two-dimensional flow. It is a time-discrete stretch and fold mechanism, which separates most initially neighboring particle pairs exponentially. Exponential separation of particles is the key signature of chaotic advection. Incompressible or area preserving means that one region is mapped onto another region of equal area. This is in contrast with the classical baker map, which is contractive, i.e., one region gets mapped onto a smaller region. The classical baker map therefore exhibits a strange attractor [11], whereas the incompressible baker map produces a space filling advected scalar as is also the case of other chaotic incompressible flows [12]. It is noteworthy that there is a difference between a two-dimensional chaotic flow and the incompressible baker map: The baker map is a discontinuous function of space, producing large scalar field gradients that generally do not exist in two-dimensional flows. However this is not significant for the following discussion because our focus will be on the effect of large-scale nonuniformities of the scalar field rather than small-scale steep scalar gradients. Figure 1 shows the baker map acting on the unit square.

The stretch and fold mechanism translates into the map

$$
\begin{pmatrix} x_n \\ y_n \end{pmatrix} \rightarrow
\begin{cases}
\begin{pmatrix} \alpha x_n \\ \dfrac{1}{\alpha} y_n \end{pmatrix}, & y_n \in [0,\alpha] \\[2em]
\begin{pmatrix} \beta x_n + \alpha \\ \dfrac{1}{\beta}(y_n - \alpha) \end{pmatrix}, & y_n \in \,]\alpha,1].
\end{cases}
\tag{9}
$$

The parameters α and β describe the degree of straining under this map. Due to incompressibility, $\alpha + \beta = 1$. We assume in this paper without loss of generality that $\alpha \leqslant \beta$. The action of the incompressible baker map on a scalar field $\Theta(x,y)$ is simply given by

$$
\Theta(x_n, y_n) \rightarrow \Theta(x_{n+1}, y_{n+1}).
\tag{10}
$$

As we want to study the scalar variance decay in a situation where the decay mechanism from AFOG96 does not occur, we consider a scalar field which is homogeneous in the y direction, the direction of the positive Lyapunov exponent. Then the map simplifies to a one-dimensional mapping of the scalar field,

$$
\Theta(x) \rightarrow
\begin{cases}
\Theta\left(\dfrac{x}{\alpha}\right): & x \in [0,\alpha] \\[1.5em]
\Theta\left(\dfrac{x-\alpha}{\beta}\right): & x \in \,]\alpha,1].
\end{cases}
\tag{11}
$$

This one-dimensional map represents the advection contribution of our model, the incompressible and diffusive baker map.

Diffusion. In order to study mixing processes, we also have to consider diffusion of the scalar field. The diffusion is modeled by carrying out a diffusion step after each advection step of the baker map. The diffusion step is described by the diffusion equation, with diffusivity κ,

$$
\frac{\partial}{\partial t}\Theta(x,t) = \kappa \frac{\partial^2}{\partial x^2}\Theta(x,t),
\tag{12}
$$

acting on the scalar field Θ for a certain time T. Note that we consider a scalar field which is homogenous in the y direction, and therefore diffusion occurs only in the x direction. At the boundaries of the unit interval, we assume periodic boundary conditions. The combination of the advection step and a subsequent diffusion step yields the incompressible and diffusive baker map, which we study in this paper. This map has already been studied in other contexts, e.g., in dynamo theory [13,14].

Fourier representation. For analytical and numerical reasons it proves useful to describe the incompressible, diffusive baker map in Fourier space. Numerically, it is easy to control the scalar diffusivity in the Fourier representation. The Fourier representation also helps to understand the scalar variance decay in terms of transport of modes through Fourier space, the so-called interscale transfer. We write the periodic scalar field Θ as a Fourier series

$$
\Theta(x) = \sum_{n=-\infty}^{\infty} \Theta_n e^{i2\pi nx}.
\tag{13}
$$

Each Fourier coefficient Θ_n is characterized by its mode number n which is related to a wave number by $k = 2\pi n$. The Fourier coefficients can be calculated from the scalar field using

$$
\Theta_n = \int_0^1 dx\, \Theta(x) e^{-i2\pi nx}.
\tag{14}
$$

The incompressible baker map (11) with diffusion (12) is a linear map and can therefore be written as a matrix acting on the Fourier coefficients

$$
\Theta_n(l+1) = \sum_{m=-\infty}^{\infty} M_{nm} \Theta_m(l),
\tag{15}
$$

with $\Theta_n(l)$ being the Fourier coefficients at time step $t = lT$. The matrix M_{nm}, which we call the *transfer matrix* in the following, reads

$$
M_{nm} = e^{-4\pi^2 \kappa T n^2 - i\pi\alpha n} \frac{\sin(\pi\alpha n)}{\pi} \frac{(\beta-\alpha)m}{(m-\alpha n)(m-\beta n)}
\tag{16}
$$

for $0 \leqslant \alpha \leqslant 0.5$. If the denominator of a particular matrix element has a resonance, i.e., either $m - \alpha n = 0$ or $m - \beta n = 0$, the nondiffusive part of this transfer matrix element has the value α or β, respectively; all other matrix elements with the same n vanish. In the case where $\alpha = 0.5$, both factors in the denominator vanish simultaneously, the resonances coincide and hence the nondiffusive part of the transfer matrix is $(\alpha + \beta)\delta_{m,n/2} = \delta_{m,n/2}$. The transfer matrix conserves the reality of an advected field by fulfilling $M_{-n,-m} = M_{n,m}^*$, whereby $*$ denotes the complex conjugate. In the nondiffusive case $\kappa = 0$, the transfer matrix furthermore conserves the variance of the field, i.e., $\Sigma_k M_{k,n} M_{-k,-m} = \delta_{nm}$. Finally, we express the scalar variance $E(l) = \int dx \Theta^2(x,l) - [\int dx \Theta(x,l)]^2$ at time step l in terms of the Fourier components $\Theta_n(l)$,

$$
E(l) = 2\sum_{n=1}^{\infty} |\Theta_n(l)|^2.
\tag{17}
$$

Analytical solutions. In the two special cases, $\alpha = 0$ and $\alpha = \frac{1}{2}$, it is relatively straightforward to find an analytical solution for the evolution of the Fourier coefficients and an analytical form for the scalar variance decay. When $\alpha = 0$, no straining occurs and we are therefore left with pure diffusion of the initial modes. Assuming a sin-wave with period 1 as initial condition, i.e., all $\Theta_n = 0$ except $\Theta_{\pm 1} = \mp i/2$, we find an exponential scalar variance decay

$$
E(l)|_{\alpha=0} = E(0)\exp(-8\pi^2 \kappa T l).
\tag{18}
$$

When $\alpha = \frac{1}{2}$, the number of modes does not increase under subsequent mappings. Instead, there is only one mode with

increasing wave number $k(l)=2\pi 2^l$. The decay of this mode with amplitude 1 yields a superexponential decay of the scalar variance

$$E(l)|_{\alpha=0.5}=E(0)\exp\left(-\frac{32}{3}\pi^2\kappa T(4^l-1)\right). \quad (19)$$

In comparison with the decay for $\alpha=0$, the above decay for $\alpha=\frac{1}{2}$ is much faster, which is due to the exponential transport of modes to higher wave numbers where they can decay very fast. (This superexponential decay is also observed in related dynamo models, see, for example, Eq. 3.1.8 in Ref. [15].)

Numerical solutions. For $0<\alpha<\frac{1}{2}$, it proves difficult to find an analytical solution of the incompressible diffusive baker map. Nevertheless we can find numerical solutions of Eq. (15) and gain an insight into the mechanisms responsible for scalar variance decay. The numerical solutions are calculated from a truncated transfer matrix. The diffusive contribution $\exp(-4\pi^2\kappa Tn^2)$ of the transfer matrix (16) makes all modes with $|n|\gg n_d$ negligible,[2] where

$$n_d=\frac{1}{2\pi\sqrt{\kappa T}} \quad (20)$$

is a diffusive cutoff. It is therefore sufficient to consider only transfer matrix elements up to N with $N\gg n_d$. The truncated matrix approximates well the behavior of the transfer matrix. We have checked that with increasing truncation number, the results of matrix iterations quickly converge. Our simulation employed up to 2048 Fourier modes, which allowed diffusivities as small as $\kappa T=10^{-8}$. Figures 2 and 3 show, respectively, the short- and long-time behaviors of the numerically obtained variance decay. For short times, i.e., $l<l_c$ in Fig. 2 (the crossover time l_c is determined in Sec. III), we observe that, initially, the variance decays hardly at all, but then within only only a few iterations almost all the variance is very quickly lost. AFOG96 referred to this decay range as the initial transient. The initial transient is followed by the final decay range where, see Fig. 3, the remaining few percent of the variance decay exponentially on average [2,3] with superimposed oscillations [4]. For small enough diffusivities, the average value of $(d/dl)\ln E$ does not appear to significantly depend on diffusivity, see Fig. 3(a). Furthermore, we observe that the larger α, i.e., the more nonuniform the map, the slower the variance decays, see Fig. 3(b). These last three observations are investigated in more detail in Secs. IV and V.

III. THE INITIAL TRANSIENT

In this section we discuss the initial transient of the scalar variance decay. Note that the properties of the scalar spectrum during the initial transient were extensively discussed in AFOG96. Here we derive an analytical approximation to

---

[2]The only exception is the case $\alpha=\frac{1}{2}$ where the high wave-number modes are the sole contribution to the variance.
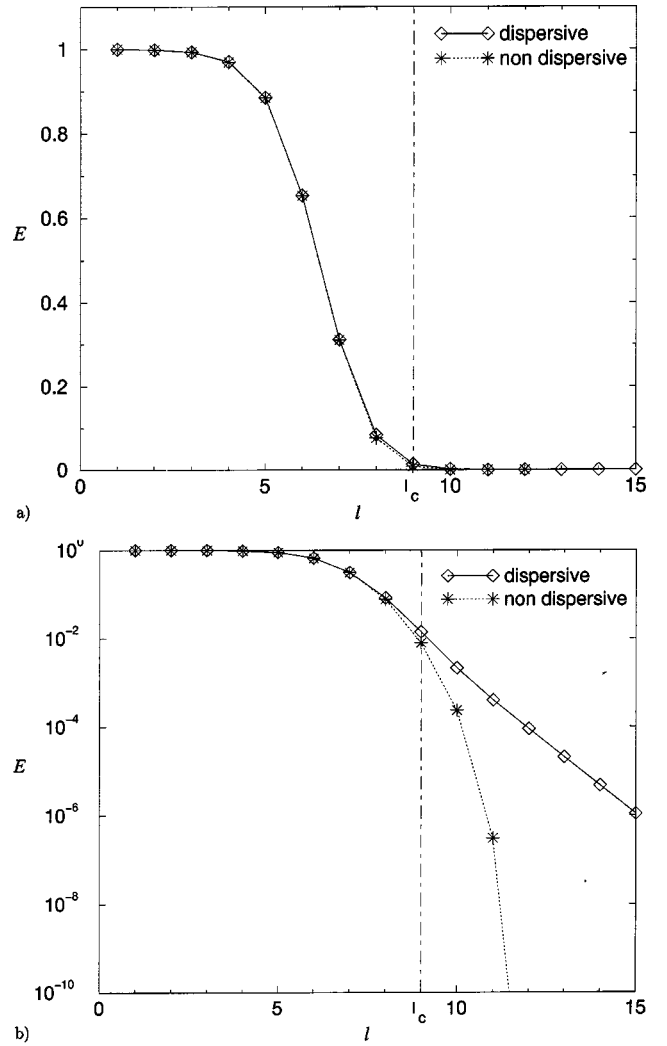
FIG. 2. Initial transient of the incompressible and diffusive baker map. Scalar variance E decay under the incompressible and diffusive baker map ($\diamond$ dispersive) and the $\alpha\beta$ map (* nondispersive) introduced in Sec. IV. Both maps have parameters $\alpha=0.4$ and $\kappa T=10^{-6}$. (a) The incompressible and diffusive baker map and $\alpha\beta$ map have the same decay as long as $l\lesssim l_c$, where l_c is given in Eq. (28). (b) For $l>l_c$, the scalar variance decays exponentially under the incompressible and diffusive baker map; however it decays superexponentially under the $\alpha\beta$ map.

the variance decay using the star equation from Sec. I and assuming constant strain history in the case of the incompressible and diffusive baker map.

Variance decay and Lyapunov exponents. The successful applications of the star equation (*) in Sec. I for long-time variance decay in fully chaotic and vortical flows motivate us to investigate its applicability in the context of the initial transient decay in fully chaotic flows. In our model, the angle ϕ between the scalar gradients and the direction of the fastest growing particle separation is $\phi=\pi/2$. Assuming, similarly to the derivation of Eq. (6), a constant strain history for all particle pairs, the integration over space in (*) can be replaced by an integration over the distribution $\mathcal{P}(h,l)$ of finite time Lyapunov exponents h (see AFOG96 for a defini-
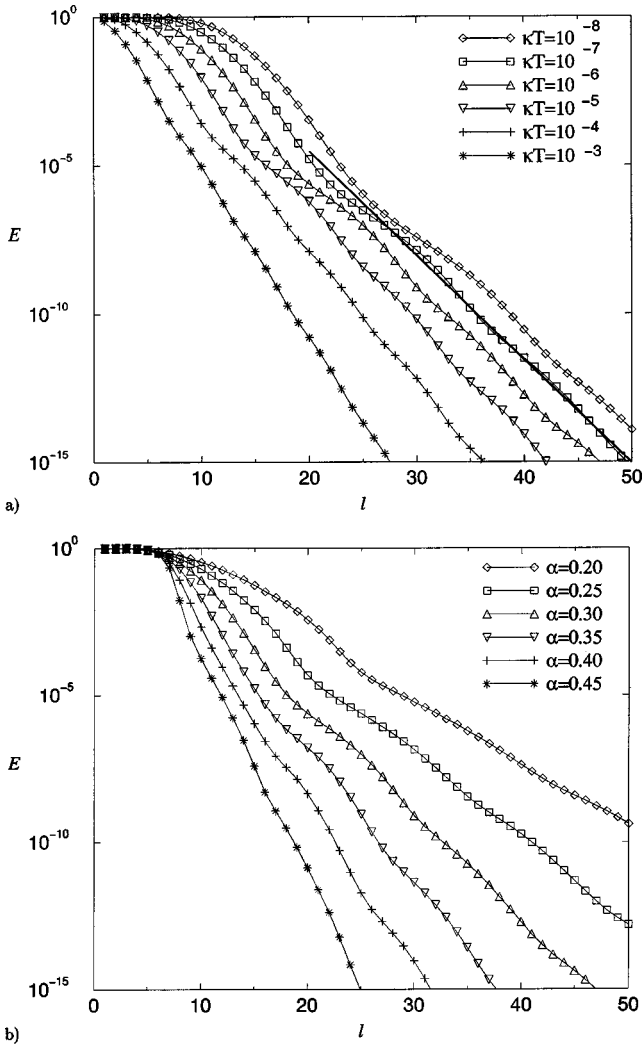
FIG. 3. Semilogarithmic plot of scalar variance E as a function of time-iteration l. (a) $\alpha = 0.3$; six different diffusivities κT ranging from 10^{-8} to 10^{-3} (number of Fourier modes $N = 2048$); decay according to the largest modulus eigenvalue (30) of the truncated transfer matrix ($N = 256$) is indicated by the thick solid line. Note that the average value of $(d/dl)\ln E$, corresponding to the average slope of the plots, appears independent of diffusivity for small enough diffusivities. A more detailed investigation of diffusivity dependence in Fig. 6 reveals that the decay factor depends at most like $\ln \kappa T$ on the diffusivity. Note also that the average decay factor is well described by the largest eigenvalue modulus of the truncated transfer matrix. (b) $\kappa T = 10^{-6}$ (number of Fourier modes $N = 512$); six different parameters α ranging from 0.2 to 0.45. Note that the larger the value of α, the faster is the decay. This means that the decay is slower when the map is less uniform. In both graphs, the averaged decay rate is overlaid with oscillations. Refer to Sec. IV for an explanation in terms of the pair of complex conjugate eigenvalues.

tion of finite time Lyapunov exponents) at time-iteration l. We make for a_0 the same choice as AFOG96, that is, $a_0 = L\Delta_0$ where we chose L to be $1/2\pi$ (this choice ensures the correct result for a plane wave scalar field with period 1 subject to uniform and constant strain, which is a reference case for our initial condition). The star equation becomes

$$E(l) = E(0) \int_0^\infty dh \mathcal{P}(h,l) \exp\left(-\frac{4\pi^2 \kappa T}{h}(e^{2hl} - 1) \right).$$
(21)

AFOG96 have used the star equation to derive scalar variance decay in the long-time limit. Here we use Eq. (21) that is derived from the star equation with an assumption of constant strain history to calculate the variance decay in the initial transient.

Analytical approximation to the variance decay. In order to estimate the variance decay from Eq. (21), we introduce the cutoff diffusion approximation and also use a Gaussian approximation for the distribution of Lyapunov exponents. The expression (21) for the variance decay can be greatly simplified by the cutoff diffusion approximation. If the argument $4\pi^2 \kappa T \exp(2hl)/h$ of the first exponential in Eq. (21) is much smaller than $\frac{1}{2}$, the value of this exponential is very close to one. However if the argument is much larger than $\frac{1}{2}$, the exponential vanishes. (Note that we have assumed $e^{2hl} \gg 1$, which is reasonable for sufficiently small κT.) The ratio $E(l)/E(0)$ is therefore approximately equal to the integral of the distribution of finite time Lyapunov exponents over a range bounded from above by a cutoff value h_c where this exponential abruptly jumps from one to zero. The value of this cutoff can be estimated by setting the argument of the exponential equal to $\frac{1}{2}$ and approximating the $1/h$ contribution of the argument by the average value $2/(h_\alpha + h_\beta)$, where $h_\alpha = -\ln \alpha$ and $h_\beta = -\ln \beta$ are the Lyapunov exponents corresponding to uniform straining by α and β respectively:

$$h_c(l) = \frac{1}{2l} \ln \frac{h_\alpha + h_\beta}{16\pi^2 \kappa T}.$$
(22)

Now we turn to approximating the distribution of finite time Lyapunov exponents. For the incompressible baker map, this distribution is given by [16]

$$\mathcal{P}(h,l) = \sum_{n=0}^l \binom{l}{n} \alpha^{l-n} \beta^n \delta\left(h - h_\alpha + \frac{n}{l}(h_\alpha - h_\beta) \right).$$
(23)

In the vicinity of the maximum

$$h_{max} = \tfrac{1}{2}(h_\alpha + h_\beta) - \tfrac{1}{4}(h_\alpha - h_\beta)^2$$
(24)

of the distribution, the binomial coefficient

$$\binom{l}{n}$$

multiplied by $\alpha^{l-n}\beta^n$ can be approximated by a normal distribution

$$\mathcal{P}(h,l) \approx \sqrt{\frac{2l}{\pi(h_\alpha - h_\beta)^2}} \exp\left[-2l\left(\frac{h - h_{max}}{h_\alpha - h_\beta} \right)^2 \right].$$
(25)

Note that this is a valid approximation during the initial transient because, as we determine below, the initial transient is the range of times where the scalar variance decay is deter-
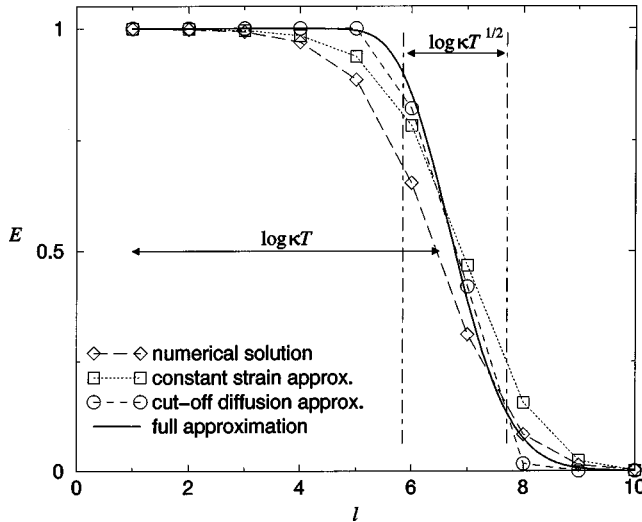
FIG. 4. Comparison of full direct numerical calculation of the variance decay under the incompressible and diffusive baker map with the approximation (26). The scaling with diffusivity κT of the time needed for most of the decay to occur, and of the temporal width of the decay region, are indicated by solid arrows. Intermediate approximations such as the Lagrangian approach based on the star equation and Lyapunov exponents (which assumes a constant strain history) leading to Eq. (21), the cutoff diffusion approximation that uses Eq. (22) and the full approximation (26) that also uses the Gaussian form of the distribution of Lyapunov exponents are also given. The parameters of the simulation are $\kappa T = 10^{-6}$ and $\alpha = 0.4$, yielding $l_c = 9$, i.e., the approximations are valid up to iteration 9.

mined by the Lyapunov exponents in the vicinity of the maximum rather than the tails of the distribution of finite time Lyapunov exponents. Integrating $\mathcal{P}(h,l)$ as given by Eq. (25) over h in cutoff diffusion approximation (22), we obtain the estimate

$$E(l) = E(0)\mathrm{erf}\left[\sqrt{4l} \, \frac{h_c(l) - h_{max}}{h_\alpha - h_\beta} \right] \qquad (26)$$

for the decay of scalar variance during the initial transient, where

$$\mathrm{erf}(x) = \frac{1}{\sqrt{2\pi}} \int_{-\infty}^{x} dy \, \exp\left(-\frac{y^2}{2} \right) \qquad (27)$$

is the error function.

Discussion of approximation. Figure 4 shows a comparison of $E(l)$ obtained by a full numerical solution of the incompressible and diffusive baker map and the approximation (26). We observe satisfactory agreement between the numerical solution and our analytical approximation suggesting that it is sufficient to know the Lyapunov exponents, a Lagrangian property of the chaotic flow, for a satisfactory description of the variance decay during the initial transient. The approximation (26) is valid as long as most of the variance has not yet decayed, see Sec. IV. Most of the variance has decayed when the cutoff for the Lyapunov exponents

(22) is smaller than the smallest Lyapunov exponent h_β. Therefore for iterations $l > l_c$, where

$$l_c = \frac{1}{2h_\beta} \ln \frac{h_\alpha + h_\beta}{16\pi^2 \kappa T}, \qquad (28)$$

which is derived from $h_\beta = h_c(l_c)$, the approximation (26) to the variance decay is not valid any longer. We have verified numerically in a variety of cases (different values of α and κT) that l_c is indeed the crossover time in Fig. 2 and that Eq. (26) is a good approximation for $E(l)$ in the initial transient range that is bounded from above by a time of order l_c. (The logarithmic dependence of a critical mixing time such as l_c has already been noted in previous studies, e.g., Ref. [17].)

Dependence on diffusivity. When the diffusivity κT changes, the time dependence of the variance changes in two ways. For smaller κT, the time around which most of the variance suddenly decays increases, but very slowly, in fact proportionally to $-\ln \kappa T$. This follows, for example, from Eq. (28). The number of time iterations required for this sudden decay to happen also increases with decreasing κT, but even more slowly. A quick calculation based on Eq. (26) shows that the width of the decay region scales like $\sqrt{-\ln \kappa T}$. The initial transient decay regime of a scalar advected by a fully chaotic flow appears, therefore, to be a case where the dissipation rate is not independent of diffusivity but where this dependence is extremely weak, in fact logarithmic.

IV. THE LONG-TIME EXPONENTIAL DECAY

In this section we begin with reviewing the explanation of long-time exponential variance decay in terms of eigenvalues of the transfer matrix and dispersion of modes [10]. This explanation serves as a foundation for the remainder of this paper, where we explain the variance decay in terms of large-scale nonuniformities of the map.

Exponential decay for long-times. In the final decay range, $l \gg l_c$, the variance decay cannot be captured by a purely Lagrangian description based on the star equation and Lyapunov exponents. Calculating the long-time decay from the star equation in the guise of Eq. (21) with Eq. (23), we find a superexponential variance decay. This calculation obviously disagrees with the numerical results of Sec. II, which suggest an exponential variance decay when $\alpha \neq 0.5$ in the long-time limit, see Fig. 3. As discussed in Sec. I, it is the additional integration over different orientations of the scalar gradient in the star equation that produces the exponential decay obtained by AFOG96. However, we have deliberately chosen the initial conditions such that all scalar gradients are aligned with the inward straining and therefore no such averaging effect applies in our case.

Final decay in terms of eigenvectors and values. Let us first explain the observed long-time exponential variance decay and its oscillations in terms of eigenvectors and eigenvalues of the truncated transfer matrix (16), see also Ref. [10]. For each eigenvalue λ with eigenvector e_n the truncated transfer matrix also has the complex conjugate eigen-
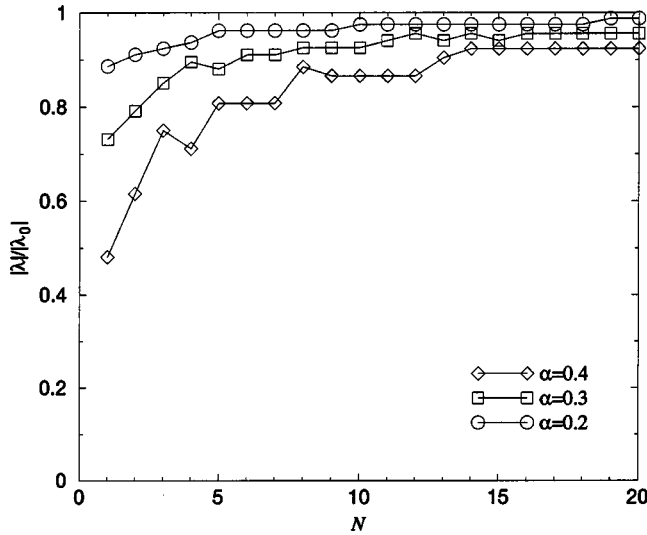
FIG. 5. Convergence of the largest eigenvalue modulus $|\lambda|$ with increasing truncation N for different α. $|\lambda|$ is calculated from a numerical eigenvalue analysis of the truncated transfer matrix. It is compared with the largest eigenvalue modulus reference value $|\lambda_0|$ that is calculated from a direct numerical solution of the variance decay, i.e., the $|\lambda_0|$ are the square roots of the decay rates in Table I. We observe that even for small values of N (particularly when α is small), the largest eigenvalue modulus $|\lambda|$ comes close to the reference value $|\lambda_0|$.

value $\lambda*$ with eigenvector $\tilde{e}_n := e^*_{-n}$. This is a consequence of the conservation of reality, $M_{-n,-m} = M^*_{n,m}$, of the transfer matrix. After a few iterations, the eigenvectors with the largest modulus eigenvalues provide the largest contribution to the scalar field and therefore control the scalar field decay in the long term. At every iteration step l, the eigenvectors are multiplied by their corresponding eigenvalues leading to the long-time approximation

$$\Theta_n(l) \approx \lambda^l e_n + \lambda^{*l} \tilde{e}_n, \qquad (29)$$

where λ and $\lambda*$ now symbolize the two largest modulus eigenvalues and e_n, $\tilde{e}_n$ their respective eigenvectors. We calculate the variance decay using Eq. (17) and find an exponential decay superimposed on a potentially oscillatory contribution:

$$E(l) \propto |\lambda|^{2l} + \sum_{n=1}^{N} \text{Re}(\lambda^{2l} e_n e_{-n}), \qquad (30)$$

where Re gives the real part of its argument. The averaged decay factor $E(l+1)/E(l)$ is therefore given by $|\lambda|^2$ (after oscillations have been averaged out). The oscillations stem from the projection of the powers of the complex eigenvalue onto the real axis and can be observed in Fig. 3. They are not only present in the incompressible and diffusive baker map, but also in other chaotic flows [4]. Furthermore, the averaged decay factor does indeed appear to be well approximated by the modulus of the largest modulus eigenvalues of the truncated transfer matrix even for rather small values of the truncation N, see Fig. 5. The fact that this agreement occurs even
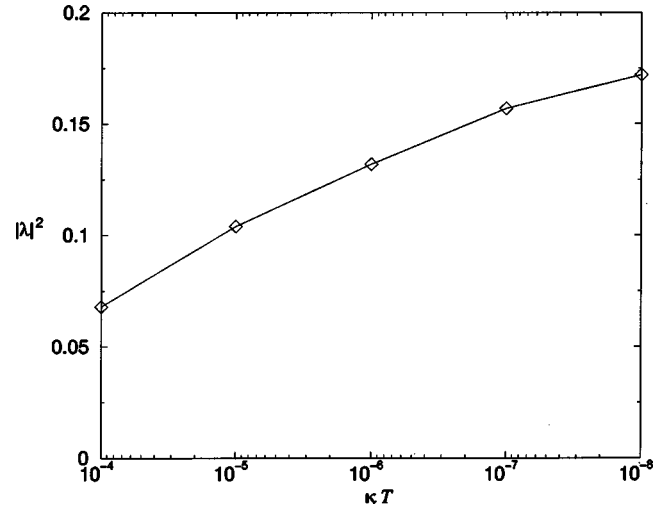
FIG. 6. Variation of the decay factor $|\lambda|^2$ with diffusivity κT in the case $\alpha = 0.475$ that is the case where $|\lambda|^2$ varies the most with diffusivity. The decay factor varies with κT slightly less steeply than $\ln \kappa T$.

for small values of N is important because it implies that it is not the discontinuities in the scalar field generated by the incompressible and diffusive baker map that are responsible for the exponential decay. Such discontinuities require many wave numbers to be resolved, more than a truncation with $N = 5$ or 10 would permit in most of our cases where the diffusivity is very small.

Parameter dependence of decay. In Fig. 3(a) we observe that for small enough diffusivities, the time derivative of the logarithm of $E(l)$ seems to become independent of diffusivity. A more detailed investigation in Fig. 6 reveals that the averaged decay factor depends at most like $\ln(\kappa T)$ on diffusivity. The average decay factors for different α are given by the "diamonds" $\diamond$ in Fig. 7 and in Table I. We observe that the larger α, i.e., the more nonuniform the map, the smaller the decay factor.

Although this simple analysis in terms of eigenvalues can predict the exponential long-time decay of the variance, it nevertheless fails to explain why a Lagrangian description based on the star equation fails and why the decay factors are so weakly dependent on diffusivity. The remainder of this section addresses this issue.

Dispersion causes exponential decay. The Lagrangian description of variance decay fails because it does not take into account the dispersion of modes during the mapping process which becomes very important after the initial transient. By dispersion[3] we mean that the transfer matrix M_{nm} does not simply map a scalar mode, characterized by its mode number m, to a single other mode n as a description in terms of

_____

[3]Note that this concept of dispersion must not be confused with a distribution of finite time Lyapunov exponents, which may also cause a transfer of variance from one mode to several other modes. In the case of finite time Lyapunov exponents, the "dispersion" of modes is caused by a local spatial average whereas our definition of dispersion considers the entire flow.
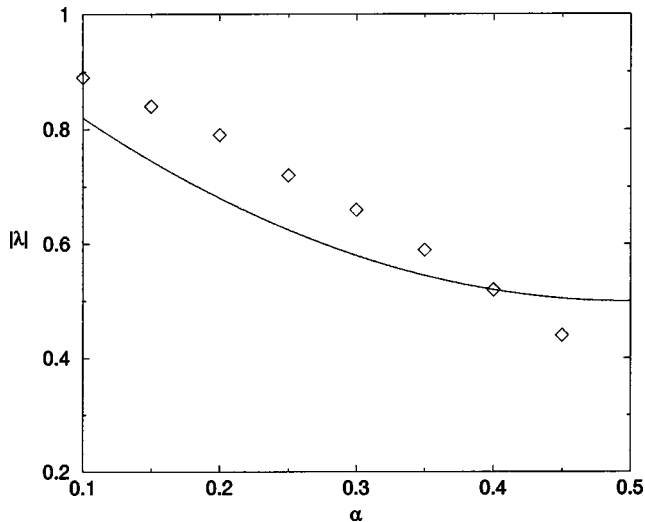
FIG. 7. Modulus of scalar field largest modulus eigenvalue $|\lambda|$, i.e., square root of the averaged decay factor $|\lambda|^2$, for different straining rates α. $\diamondsuit$, Eigenvalues obtained by a numerical solution of the incompressible and diffusive baker map with diffusivity $\kappa T = 10^{-6}$; solid line, analytical solution (44) for the eigenvalue in the Gaussian description without boundary corrections, see Sec. V B. In both cases, the eigenvalues decrease with increasing α. However, the decay behaviors are different because the corresponding maps have different large-scale nonuniformities, see Secs. IV and V. The eigenvalues are also given in Table I.

Lyapunov exponents would suggest, but instead maps mode m onto an entire distribution of modes. See, for instance, Fig. 8 for a schematic illustration of the concept of dispersion and an example of dispersion for the incompressible and diffusive baker map. Generally most of the variance contained in the initial mode m is transported to larger mode numbers. However, dispersion may cause a small fraction of the initial variance to be transferred to the same or even lower mode numbers than m. This remnant amount of variance can be quantified by the remnance $R(m)$, which is defined as the sum of contributions to the variance, which end up at the same or lower mode numbers after one iteration:

TABLE I. Square root of the averaged decay factors (oscillation averaged out), i.e., eigenvalue moduli, for the incompressible and diffusive baker map $\lambda|_{std}$ and the diffusive baker map in the Gaussian description without boundary corrections $\lambda|_{Gauss}$, see Eq. (44). The values of the incompressible and diffusive baker map are obtained by an exponential fit to the numerically calculated decay for $\kappa T = 10^{-6}$.

α	$\lambda|_{std}$	$\lambda|_{Gauss}$
0.45	0.44	0.51
0.40	0.52	0.52
0.35	0.59	0.55
0.30	0.66	0.58
0.25	0.72	0.63
0.20	0.79	0.68
0.15	0.83	0.76
0.10	0.89	0.82

$$R(m) = 2 \sum_{n=1}^{m} |M_{nm}|^2. \qquad (31)$$

Figure 9 shows the remnance of the incompressible and diffusive baker map for different α. We observe that the remnance scales like $R(m) \propto m^{-1}$ for large m, which can also be verified analytically. Due to this scaling, the remnance is only important for the lowest modes.[4] This suggests that at every iteration step, there exists a fraction of variance that remains at the lowest modes. It is this remnant fraction of variance that causes the exponential variance decay, i.e., the lowest modes control the exponential variance decay. This remnant fraction must be equal to $|\lambda|^2$ because the variance decay occurs by multiples of $|\lambda|^2$ [see Eq. (30) with averaged out oscillations]. The remaining fraction $1 - |\lambda|^2$ of variance, originally contained in the lowest modes, gets at each iteration step transported to larger wave numbers. So it finally reaches high enough wave numbers where diffusion can eliminate the variance.

Decay factor independent of diffusivity. The dispersion (remnance) decay mechanism also explains qualitatively why the decay factor becomes nearly independent of or at least extremely weakly dependent on diffusivity when diffusivity is small enough. This mechanism operates only at the largest scales of the flow. A small diffusivity, however, only acts at much smaller scales and can therefore not influence the decay factor very much.

Lyapunov exponents fail because of lacking scale separation. Considering that the exponential variance decay is controlled by the largest scales of the flow, it is not surprising that the Lagrangian description based on the star equation and Lyapunov exponents fails to describe the exponential variance decay. As we have pointed out in Sec. I, this approach based on particle pair separation can predict variance decay when the spatial scales over which the flow varies are much larger than the scales over which the scalar field varies. This condition ceases to be fulfilled for the incompressible and diffusive baker map in the long-time limit beyond the initial transient.

$\alpha\beta$ map. To emphasize the role of mode dispersion, let us investigate fully chaotic maps without mode dispersion. As a first example, consider the incompressible and diffusive baker map for $\alpha = 0.5$. The transfer matrix (16) in this case is nondispersive and therefore produces superexponential variance decay (19). We obtain a second example of a nondispersive map by constructing a map with the same straining properties as the incompressible and diffusive baker map but no mode dispersion. Analyzing the transfer matrix (16), we see that it has resonances, i.e., comparatively large values whenever $m - \alpha n \approx 0$ or $m - \beta n \approx 0$. If a resonance condition is met exactly, the corresponding matrix element takes the value α or β, respectively. These resonances lead to a

---

[4]The importance of the lowest modes can also be inferred from the first few elements of the transfer matrix. The eigenvalues of the truncated transfer matrix quickly converge towards the measured value of variance decay, see Fig. 5.
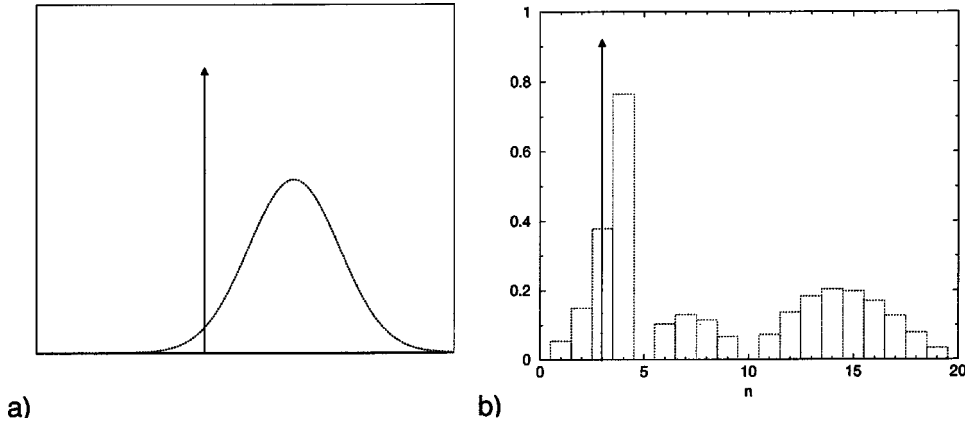
FIG. 8. Dispersion of modes. (a) Schematic illustration of dispersion with wave numbers ofthe x and intensity on the y axis. A sharp distribution of wave numbers (indicated by the vertical arrow) is mapped onto a broad distribution of modes (indicated by dotted line). (b) Dispersion of the baker map: Modulus of transfer matrix elements for $\alpha=0.3$ and vanishing diffusivity. A mode with mode number m $=3$ is mapped onto a broad distribution of modes, indicated by dotted lines.

transport of modes to higher wave numbers, i.e., a mode with wave number k and amplitude A is mapped approximately to two modes with wave numbers k/α and k/β and amplitudes αA and βA, respectively. When the resonance condition is not met precisely, the resonance is smeared out and therefore the transport of modes is dispersive. A simplified version of the incompressible and diffusive baker map is therefore obtained by assuming that the transfer matrix has only sharp resonances, i.e., nondispersive transport of modes. In the following we refer to this nondispersive baker map as the $\alpha\beta$ *map*. Introducing a continuous mode distribution $P(k)$, the evolution of $P(k)$ under the $\alpha\beta$ map is given by

$$P(k)\rightarrow D(k)[\alpha P(\alpha k)+\beta P(\beta k)], \qquad (32)$$

where the diffusive factor $D(k)$ models diffusion. From the diffusive term $\exp(-4\pi^2\kappa Tn^2)$ in Eq. (16), we infer $D(k)=\exp(-\kappa Tk^2)$. Figure 2 compares scalar variance decay un-

FIG. 9. Double-logarithmic plot of remnance R over mode number m for $\alpha=0.2$, 0.3, 0.4, and 0.45. The dashed line indicates $1/m$ scaling. The remnance is larger for smaller α at any m, and for large m the remnance decays like $1/m$.

der the incompressible and diffusive baker map and the $\alpha\beta$ map. As long as the majority of modes is not transported beyond the diffusive cutoff, i.e., $l<l_c$, both maps evolve almost identically. However for $l>l_c$ the incompressible and diffusive baker map and the $\alpha\beta$ map evolve differently. The incompressible and diffusive baker map develops an exponential decay but the $\alpha\beta$ map decays superexponentially. We expect these results because the incompressible and diffusive baker map is dispersive whereas the $\alpha\beta$ map is not. Note that the $\alpha\beta$ map is very similar to the Lagrangian decay description (21) in terms of Lyapunov exponents derived from the star equation. The sole difference between the two descriptions is that the $\alpha\beta$ map does not require the assumption of constant strain. Therefore the variance decay calculated with the $\alpha\beta$ map in Fig. 2 agrees even better with the full numerical solution than the decay according to the Lyapunov description (21) in Fig. 4.

Dispersion and large-scale nonuniformity of the straining field. Having established that dispersion causes the exponential variance decay of the incompressible and diffusive baker map in the first place, we now argue that dispersion itself is caused by the nonuniformity of the advecting flow or map. In the case where $\alpha=0.5$ the straining of the map is uniform and produces a uniform scalar field. This is also the one case where the incompressible and diffusive baker map is not dispersive. However, as α decreases away from 0.5, the straining field of the map becomes increasingly nonuniform and hence the map also because increasingly dispersive, as measured by the remnance which increases with decreasing α. Clearly, dispersion and nonuniformity appear to be correlated in the case of the incompressible and diffusive baker map. But could there be a causal relation between the two which might be valid quite generally over a wide class of flows? We investigate this question by comparing maps that have the same straining properties but are differently organized in space. The dispersion by such maps can be analyzed by means of the Fourier transforms of the scalar fields that they produce. Figure 10 shows two examples of scalar fields that are produced by maps with identical straining properties so
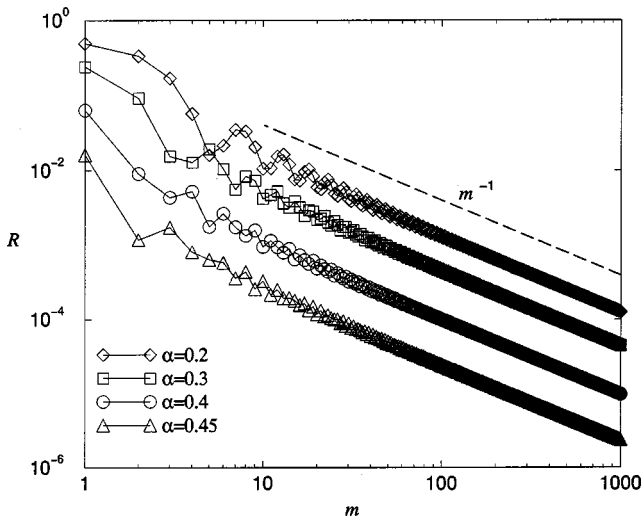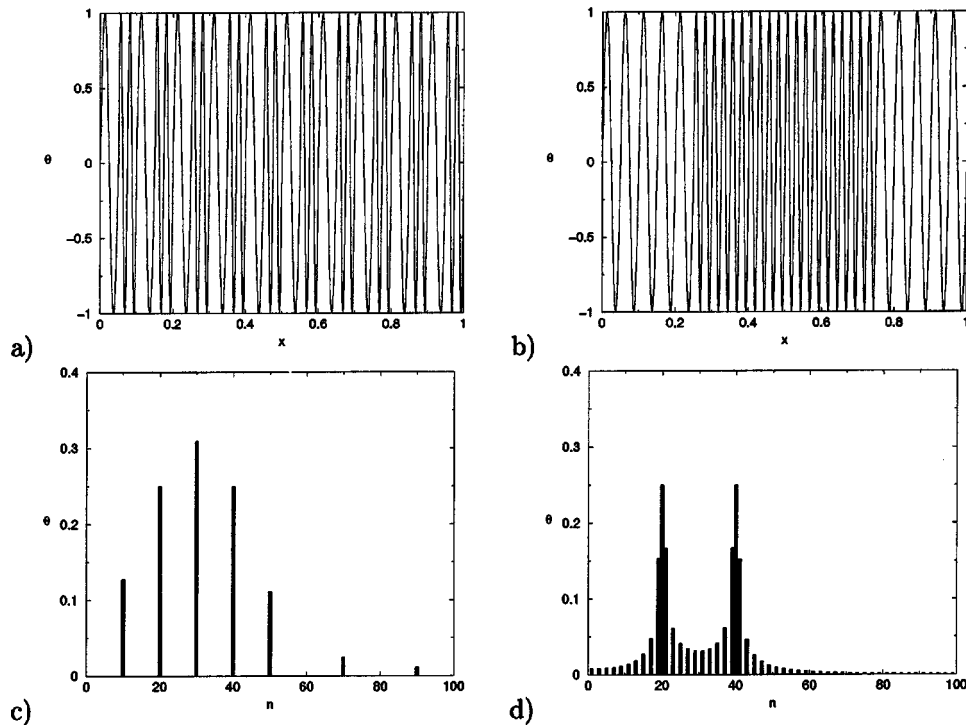
FIG. 10. Scalar field made up of ten sine waves with wave number $2\pi \times 20$ and 20 sine waves with wave number $2\pi \times 40$. (a) The waves are arranged such that they are uniform on a large scale, (b) the waves are arranged such that they are nonuniform on a large scale, (c) Fourier transform of (a), (d) Fourier transform of (b). The more nonuniform field (b) has a more dispersive spectrum.

that both scalar fields have the same subfield components of truncated sine waves. However the spatial arrangement of subfield components is different for both maps. The field in Fig. 10(a) is more uniform than the field in Fig. 10(b) because all large scale sections in (a) are comparable, whereas in (b) different kinds of large-scale sections can be found. The Fourier representation of field (a), see (c), is less dispersive, i.e., has narrower peaks around the maxima, than the Fourier components of field (b); see (d). Indeed our example of Fig. 10 suggests that there is a general causal relation between spatial nonuniformity of a map (and consequently that of its advected field) and dispersion of interscale transfer. Note that Pedrizetti and Vassilicos [18] have described scalar interscale transfer in vortical flows in terms of a transfer matrix, which is also dispersive, and have found a similar relation between the dispersion caused by the transfer matrix and the spatial nonuniformity of the shear field in the vortex.

V. GAUSSIAN DESCRIPTION OF CHAOTIC MAPS

The large-scale nonuniformities of a chaotic map influence the long-time variance decay of the map. To illustrate this point further, we introduce the Gaussian description of the incompressible and diffusive baker map. Using the Gaussian description, we can show that two chaotic maps with, for the intents and purposes of this paper, identical distributions of finite time Lyapunov exponents but different large-scale nonuniformities have different long-time variance decay rates. The first map, the Gausian description of the incompressible and diffusive baker map of the previous sections, is discussed in Sec. V A. We show that the Gaussian description reproduces the variance decay. In Sec. V B, we proceed by introducing a second map which, in comparison with the incompressible and diffusive baker map, has differ-

ent large-scale nonuniformities but the same distribution of finite time Lyapunov exponents. Changing the large-scale nonuniformities while keeping the distribution of Lyapunov exponents is the key advantage of the Gaussian description and the reason why we introduce it in this section. Note that we do not introduce the Gaussian description to provide an improved algorithm to simulate advection-diffusion processes. The Gaussian description is not well suited for this task. First, its memory requirements grow exponentially with simulation time. Second, it is only applicable for one-dimensional chaotic maps. Nevertheless, the ability of the Gaussian description to describe chaotic maps with different large-scale nonuniformities but identical distributions of Lyapunov exponents allows us to show that the large-scale nonuniformities have a significant influence on the rate of variance decay.

A. Introduction of Gaussian description and application to the incompressible and diffusive baker map

Definition of Gaussian description. We introduce the *Gaussian description* of a chaotic map by studying the combined effect of strain and diffusion on a Gaussian scalar field

$$g_\sigma(x) = \exp\left(-\frac{x^2}{4\sigma^2}\right). \tag{33}$$

Any Gaussian remains a Gaussian under uniform strain and diffusion. Even if the Gaussian is subject to nonuniform strain, it quickly returns to its initial shape under the influence of diffusion. (We have verified that the bell-shaped curves in Fig. 11(c) are well fitted by Gaussians). Therefore Gaussians are convenient for the study of chaotic maps. As an example, we study the incompressible and diffusive baker

a)

b)

c)
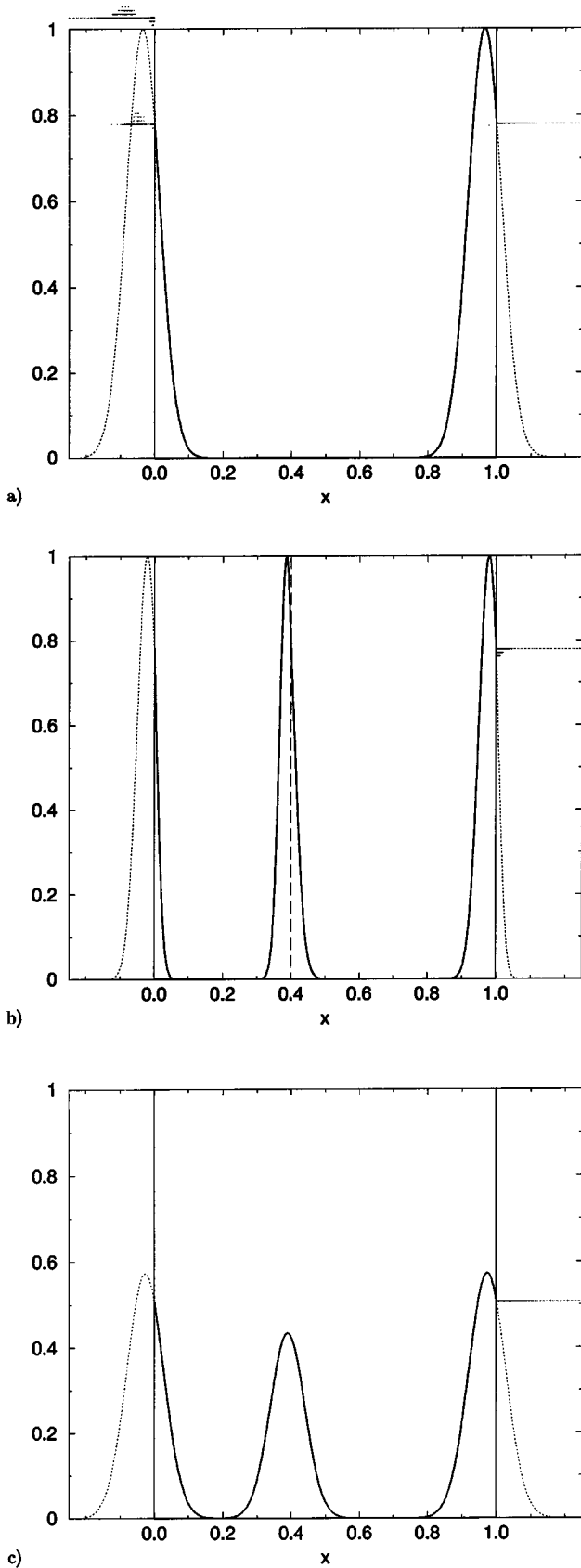
FIG. 11. Evolution of Gaussians in the vicinity of the boundary. Field Θ plotted against position x.

map (11) and (12) in the Gaussian representation. Assume an incompressible and diffusive baker map with a Gaussian initial condition

$$\Theta(x,0)=A_1^{(0)}g_{\sigma_1^{(0)}}(x-x_1^{(0)})-\bar{g}. \tag{34}$$

Our initial condition is characterized by the amplitude $A_1^{(0)}$, by the width $\sigma_1^{(0)}$ (which shall be much smaller than 1, the size of the mapped interval), and by the peak center $x_1^{(0)}$ (which shall be well inside the mapped unit interval). The mean $\bar{g}$ is subtracted to obtain a field with vanishing average.[5] We assume that this specific initial condition has no influence on the character of the long-time decay.

Uniform Gaussian description. Consider the application of one iteration step of the incompressible and diffusive baker map and assume, for the time being, that the Gaussian remains well inside the mapped interval. First, one peak is mapped on two peaks: one peak resulting from a compression with α and the other from a compression with β. Then, diffusion acts for a time T and the peaks become wider and lower. Hence, at every iteration, one Gaussian is mapped on two new Gaussians with modified amplitudes, widths, and centers. Because the problem is linear, the scalar field after l iterations can be written as a superposition of Gaussians,

$$\Theta(x,l)=\left(\sum_{n=1}^{2^l}A_n^{(l)}g_{\sigma_n^{(l)}}(x-x_n^{(l)})\right)-\bar{g}. \tag{35}$$

In the Gaussian description, the field is fully characterized by the set of parameters $A_n^{(l)}$, $\sigma_n^{(l)}$, and $x_n^{(l)}$. From the definitions (11) and (12) of the incompressible and diffusive baker map, the evolution of the parameters follows, see the Appendix,

$$x_n^{(l)}\rightarrow\begin{cases}x_n^{(l+1)}=\alpha x_n^{(l)}\\x_{2^l+n}^{(l+1)}=\alpha+\beta x_n^{(l)},\end{cases} \tag{36}$$

$$A_n^{(l)}\rightarrow\begin{cases}A_n^{(l+1)}=A_n^{(l)}\left(1+\dfrac{\kappa T}{(\alpha\sigma_n^{(l)})^2}\right)^{-1/2}\\A_{2^l+n}^{(l+1)}=A_n^{(l)}\left(1+\dfrac{\kappa T}{(\beta\sigma_n^{(l)})^2}\right)^{-1/2},\end{cases} \tag{37}$$

$$\sigma_n^{(l)}\rightarrow\begin{cases}\sigma_n^{(l+1)}=\sqrt{\kappa T+(\alpha\sigma_n^{(l)})^2}\\\sigma_{2^l+n}^{(l+1)}=\sqrt{\kappa T+(\beta\sigma_n^{(l)})^2}.\end{cases} \tag{38}$$

Studying the long-time evolution of the parameters, we find that the widths σ approach values between

$$\sigma_\alpha=\sqrt{\frac{\kappa T}{1-\alpha^2}}\quad\text{and}\quad\sigma_\beta=\sqrt{\frac{\kappa T}{1-\beta^2}}. \tag{39}$$

---

[5]In Sec. V B, we describe and discuss an alternative method to obtain a field with vanishing average.

The minimal width σ_α is given by a Gaussian which is subject to pure α strain. Similarly, the maximal width σ_β is given by a Gaussian subject to pure β strain. When the peaks have reached their final range of widths, the amplitude evolution becomes relatively insensitive to the precise value of the width. For each iteration step, the amplitude reduction factor is then comparable to the corresponding strain rates α or β. If a Gaussian is subject to a single strain rate, this is indeed the exact solution.

Large-scale nonuniformities and boundary conditions. If the straining properties of the incompressible and diffusive baker map were completely uniform or if the nonuniform straining at the boundaries of the unit interval could be neglected, the field evolution and variance decay would be given by Eqs. (36)–(38). However for the standard incompressible and diffusive baker map, where $\alpha \neq \beta$, this is not the case. At the boundaries of the unit interval, regions with different straining properties come to neighbor each other directly because of the periodicity of the flow domain. The boundaries thus feel the effect of the large-scale nonuniformities and thereby influence the rate of scalar variance decay. Below, we first study in some detail the influence of the boundary conditions of the incompressible and diffusive baker map. Then, in Sec. V B, we modify the boundary conditions and show that they have a significant influence on the variance decay.

Boundary conditions. Let us now investigate the effect of the boundary conditions on the evolution of a Gaussian. If a peak center comes within about a peak width of the left- or right-hand boundary of the mapped unit interval, the Gaussian becomes subject to strain, which is nonuniform across the width of the Gaussian. The evolution of the Gaussian's amplitude, width, and center is then different from the uniform case above. We study the case of nonuniform strain numerically. Figure 11 depicts an example of a Gaussian coming close to the boundary, where it can experience the effect of nonuniform strain. Figure 11(a) shows a Gaussian which, under subsequent β stretchings, has come close to the right-hand boundary of the unit interval at $x=1$. Due to its finite width, a fraction of the field is now outside the mapped interval. As a consequence of the periodicity of the flow domain, this fraction returns to the left-hand boundary ($x=0$). The result of the stretch step of the incompressible and diffusive baker map is plotted in Fig. 11(b). The peak section at the right-hand boundary is mapped on two new peak sections. One is strained with $\beta=0.6$ and moved by $\alpha=0.4$. It therefore remains at the right-hand boundary. The other is strained with α and hence moves directly left of $x=0.4$. The peak section at the left-hand boundary is also mapped on two new peak sections. One strained with α at the left-hand boundary and the other strained with β, directly right of $x=0.4$. Finally, diffusion κ acts for a time T, see Fig. 11(c). All cut and pasted peak sections again approach the Gaussian shape. The peak at $x \approx 0.4$ has a lower amplitude than the peaks at the boundary because most of it was subject to greater strain. However its amplitude is slightly larger than 0.4, the amplitude that corresponds to the case of uniform strain with $\alpha=0.4$. Similarly, the peak at the boundary is slightly smaller than in the uniform case due to some contri-
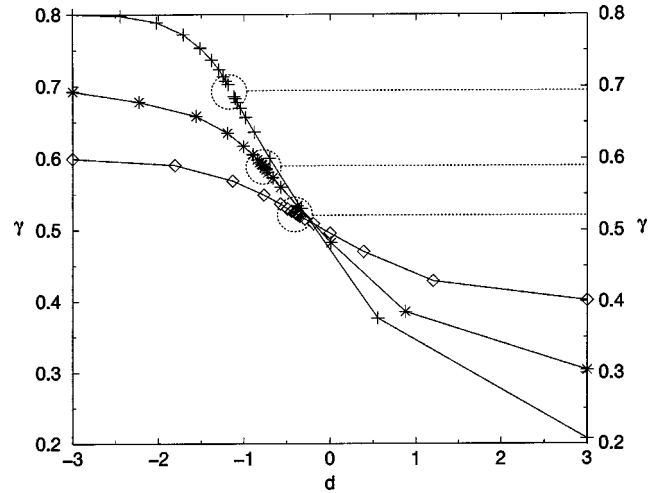
FIG. 12. Evolution of Gaussians in nonuniform strain for different strain rates. The three solid curves give the evolution of Gaussians in the strain-diffusive situation described in Fig. 11 for $\diamond$: $\alpha=0.4$; $*$: $\alpha=0.3$; $+$: $\alpha=0.2$. The Gaussian's amplitude reduction factor γ for each iteration is plotted against the Gaussian's distance d from the borderline between the regions with different strain. The distance d is measured in multiples of the Gaussian's width σ. Negative values refer to the left-hand side of the boundary, positive values to the right-hand side. Fixed points of the evolution are indicated by dotted circles with horizontal lines, from bottom to top corresponding to $\alpha=0.4$, 0.3, 0.2.

bution by the stronger α straining. The peak widths and centers also deviate from the uniform values.

Systematic study of boundary conditions for different straining rates. For other combinations of straining rates α and β, we find similar behavior. In particular, after the diffusion step, all peaks return to the Gaussian shape, even though they have been subjected to nonuniform strain. Figure 12 quantifies the effect of the Gaussian's distance from the boundary on its amplitude evolution for different combinations of straining rates. Consider the example of the incompressible and diffusive baker map with $\alpha=0.4$ and $\beta=0.6$. Let us follow the evolution of a Gaussian close to the right-hand boundary of the mapped unit interval. The amplitude reduction factor γ for one iteration of the Gaussian is given by diamonds in Fig. 12. Initially, the Gaussian is positioned three widths σ away from the boundary. The reduction factor at $d=-3$ can be read off Fig. 12, $\gamma=0.6$. This is the uniform result because the peak is far enough from the boundary. However at the next iteration step it has moved within 1.8 widths from the boundary and we begin to observe a slight reduction in the amplitude reduction factor. In the following iterations the peak gets ever closer to the boundary and the amplitude reduction factor decreases. Finally it reaches a stable distance of about 0.4 widths away from the boundary. At this fixed point the amplitude reduction factor is $\gamma=0.52$. With the same incompressible and diffusive baker map, we can also study the evolution of a Gaussian at the left-hand boundary of the unit interval. Three widths away from the boundary, we find again the uniform value for the amplitude reduction factor ($d=3$, $\gamma=0.4$). With subsequent iterations, the amplitude reduction factor in-
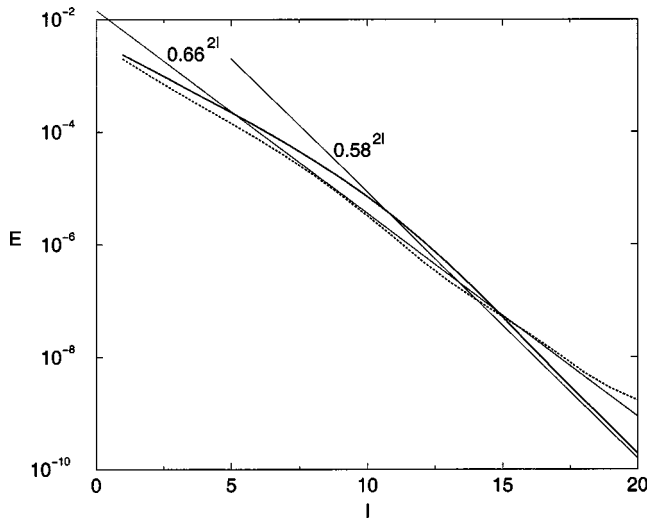
FIG. 13. Comparison of variance decay in Gaussian description with and without boundary corrections for $\alpha = 0.3$. Solid line: Decay without boundary correction. Dotted line: Decay with boundary correction; asymptotic decay rates are indicated by straight solid lines. The final range of the solution without boundary corrections decays like 0.66^{2l} according to Eq. (44). In contrast, the final range of the standard incompressible and diffusive baker map decays like 0.58^{2l}, see Fig. 7. Note that the numerical simulation of the Gaussian description is limited to a small number of iterations because the memory requirements of the simulation grow exponentially.

FIG. 14. Comparison of scalar field solutions. Solid line (upper graph): Numerical solution of the standard incompressible and diffusive baker map obtained in Fourier space and transformed to real space. Dotted line (lower graph): Numerical solution of the incompressible and diffusive baker map in Gaussian description with boundary corrections. Both solutions are calculated for $\alpha = 0.3$ and $\kappa T = 10^{-6}$ (they are rescaled and slightly displaced to allow easy comparison). We observe that both solutions have very similar structure. All spikes, whose positions can be obtained by mapping the spike at the right-hand boundary with Eq. (36), have comparable positions and amplitudes.

creases, as more and more of the peak gets subject to weaker β strain. The peak center even crosses the boundary and reaches the same fixed point. For other values of α and β, similar behavior can be observed in Fig. 12.

Comparison with numerical solution. We are now in a position to compare the solutions of the incompressible and diffusive baker map obtained by Fourier decomposition with solutions using Gaussian description, i.e., Eqs. (36)–(38) and boundary corrections from Fig. 12. We determine the time dependence of the variance decay in Gaussian description by superimposing all Gaussians in real space and then calculating the variance of the resulting fields. We observe good agreement between the variance decay in Gaussian description and the variance decay calculated from numerical solutions of the incompressible and diffusive baker map using Fourier decomposition, see Fig. 13 (the decay without boundary corrections in the figure may be omitted). Furthermore, we find by comparing the scalar fields themselves that the fields in Gaussian description are very similar to, and share the same features as, the fields calculated from the Fourier modes, see Fig. 14.

In summary, we have shown that if the following three conditions are fulfilled (see paragraph "Definition of Gaussian description"), the Gaussian description allows us to describe the evolution of the incompressible and diffusive baker map: (i) the diffusion κT is small enough so that the Gaussian widths are small in comparison with the mapped unit interval; (ii) the long-time decay does not depend on the initial condition; (iii) Gaussians under nonuniform strain can be sufficiently well approximated by the Gaussians. How-

ever, it should be noted that it is generally not useful to calculate decay factors in Gaussian approximation. The memory required to keep track of all the Gaussians grows exponentially with the number of iterations and hence quickly reaches extremely large values. The main advantage of the Gaussian description is that it enables us to change the behavior of the map at the boundary and therefore the effect of the large-scale nonuniformities.

B. Decay factor of Gaussian description without boundary conditions

Variation of boundary conditions. Instead of using the curves in Fig. 12 to describe the behavior at the boundary of the incompressible and diffusive baker map in the Gaussian description, we could imagine infinitely many different curves and therefore equally many different Gaussian descriptions with different boundary corrections. All these Gaussian descriptions have the same small-scale stretching properties (with the exception of a tiny region around the boundaries). Although the Lyapunov exponents of all those maps are the same, the decay factors are different as we show now. In particular, we study one example of such modified boundary conditions, namely the map where all Gaussians evolve according to the uniform evolution (36)–(38) and no additional corrections are considered. The advantage of this particular example is that it is analytically tractable. Note that there is no real space physical model that has these particular boundary corrections. The Gaussian de-

scription is therefore a method for changing the boundary conditions and hence the effects of large-scale nonuniformities of the incompressible and diffusive baker map.

Simplified Gaussian description. The uniform evolution (36)–(38) can be further simplified by assuming a weighted width $\bar{\sigma} = \alpha \sigma_\alpha + \beta \sigma_\beta$ for all Gaussians, where the minimal and maximal widths $\sigma_{\alpha/\beta}$ are given by Eq. (39). This approximation turns out to be a very good approximation as long as all widths are comparable, which is the case for α not too small. The uniform evolution is then given by the evolutions of the centers (36) and the approximated evolution of the amplitudes

$$A_n^{(l)} \rightarrow \begin{cases} A_n^{(l+1)} = \alpha A_n^{(l)} \\ A_{2^l+n}^{(l+1)} = \beta A_n^{(l)}. \end{cases} \tag{40}$$

Now we employ a different method to construct a field with vanishing mean. We use an initial condition of two closely neighboring Gaussians (33) whose amplitudes have the same modulus but opposite signs. The Gaussians' centers shall be only a small distance apart, in fact much smaller than the width of the peaks. We call this combination of two Gaussians a *double Gaussian*,

$$d(x) = x \exp\left(-\frac{x^2}{4\bar{\sigma}^2}\right). \tag{41}$$

The double Gaussian and all its mappings obviously have vanishing mean. Previously, we have ensured vanishing mean by simply subtracting the mean of the mapped Gaussians. The previous method has the advantage of being relatively insensitive to the correct positioning of the scalar field because all Gaussians have positive amplitude and therefore only interfere constructively. Without boundary corrections, the peak positions are known exactly. The double Gaussian representation is then advantageous because the double Gaussians amplitude corresponds directly to the amplitude of the scalar field. It is easy to show that the double Gaussian's amplitude decreases by a factor approximately equal to α^2 under α strain with subsequent diffusion step, and, similarly, by a factor approximately equal to β^2 under β strain with diffusion. This modifies the evolution of amplitudes (40) to

$$A_n^{(l)} \rightarrow \begin{cases} A_n^{(l+1)} = \alpha^2 A_n^{(l)} \\ A_{2^l+n}^{(l+1)} = \beta^2 A_n^{(l)}. \end{cases} \tag{42}$$

Analytical solution. We now derive an analytical solution for the long-time decay factor by comparing the scalar fields for subsequent iterations. We use a special initial condition, where the first double Gaussian's center is at $x_0^{(0)} = 1$. This initial condition ensures that, after one iteration, half of the Gaussians fall on positions previously occupied by Gaussians. Although we use a special initial condition to derive the decay factor, we expect our results for the Gaussian description to be independent of this specific initial condition. This expectation is motivated by the fact that the final range decay of the incompressible and diffusive baker map is insensitive to initial conditions. Almost all initial conditions of the in-

compressible and diffusive baker map contain at least an infinitely small contribution of the slowest decaying eigenmode. This contribution dominates the decay in the long run and ensures that the long-time variance decay is identical for almost all initial conditions and thus insensitive to the specific choice for the initial condition. Consider now one of the 2^l Gaussians after l iterations. It is characterized by its amplitude A_n^l and center $x_n^{(l)}$. From Eq. (42), it follows that the amplitude can be related to the binary notation of its index n, for example

$$n = 0\ 0\ 1\ 0\ 1\ 1\ \cdots\ 1,$$

$$A_n = \alpha^2\ \ \alpha^2\ \ \beta^2\ \ \alpha^2\ \ \beta^2\ \ \beta^2\ \cdots\ \beta^2. \tag{43}$$

Each 0 in the binary notation corresponds to a multiplication with α^2, and each 1 corresponds to a β^2 multiplier. The last multiplier to be applied is on the left-hand end of the binary series. After one further iteration, we have 2^{l+1} Gaussians in total. At the position of our previous Gaussian, we find a new Gaussian with amplitude $A_n\beta^2$. The direct left-hand neighbor of this Gaussian has an amplitude $A_n\alpha^2$. In the final decay range, the distance between any neighboring Gaussians is much smaller than the width of the Gaussians. We can therefore combine two Gaussians to one combined Gaussian by adding their amplitudes. We then obtain the same scalar field when adding up the combined Gaussians. The combined Gaussian has an amplitude $(\alpha^2 + \beta^2)A_n$, and we may locate it at the position x_n of the previous Gaussian. Carrying out this procedure for all the neighboring pairs of Gaussians, we find a set of Gaussians very similar to the set of Gaussians after l iterations, the only difference being that all amplitudes are reduced by a factor $\alpha^2 + \beta^2$. The field in the final decay range is hence in an eigenstate with an eigenvalue

$$\lambda = \alpha^2 + \beta^2. \tag{44}$$

This prediction for the decay factor in Gaussian description without boundary corrections can be verified by a comparison with the numerical simulations. Figure 13 shows one example of the numerical evolution which indeed matches the prediction.

Discussion. Comparing the decay factors of the standard incompressible and diffusive baker map with our solution (44) for Gaussian description without boundary corrections, see Fig. 7, we find a remarkable difference between both decay factors. This difference must be due to the different boundary corrections, because both maps are otherwise identical. As pointed out above, by modifying boundary conditions one can modify the quantitative effect of the large-scale nonuniformities of the map. In an incompressible one-dimensional map, boundaries are in fact the only place where the nonuniformities of the map can be introduced because it is here that regions with different uniform straining properties join. In conclusion, our investigation has revealed that the large-scale nonuniformities rather than small-scale straining properties determine the variance decay of a chaotic flow when the AFOG96 mechanism is not relevant. Also, the large-scale nonuniformities are responsible for the influence

of the boundary conditions on the rate of scalar variance decay and therefore for the nonuniversal value of this rate.

VI. CONCLUSION

We have studied the decay of scalar variance under the incompressible and diffusive baker map as an example of mixing in chaotic flows and maps. We have shown that the variance decay during the initial transient, i.e., the range of times when most of the variance decays, can be well described by a general relation (*) between the scalar variance decay and the particle pair separations. Using the star equation, we have even obtained an analytical approximation for the variance decay in this range of times. We have also shown that the general relation (*) explains both spiral mixing in a vortex and early time chaotic mixing as two different manifestations of the same general process.

Despite its success during the initial transient, in the final range of variance decay the star equation fails to describe the decay, at least in our model. Previously, AFOG96 used (*) successfully to explain exponential scalar variance decay in a different chaotic flow. However, for the incompressible and diffusive baker map, the star equation predicts superexponential variance decay rather than the observed exponential variance decay. Therefore we have identified a mechanism of variance decay based on dispersion/remnance, i.e., the fact that at each iteration of the map a certain amount of variance from a mode with wave number n remains at the same or smaller wave numbers. Studying two examples, we have confirmed that without dispersion/remnance, the incompressible and diffusive baker map has indeed superexponential variance decay as predicted by the star equation. The dispersion/remnance controlled variance decay also explains why the decay becomes independent of small enough diffusivity. Generally, our mechanism and the mechanism of AFOG96 coexist. The mechanism that leads to the slower decay ultimately determines the variance decay in a given chaotic flow.

Dispersion itself is caused by the large-scale nonuniformities of the flow. Introducing the Gaussian description of the incompressible and diffusive baker map, we can change the boundary conditions and thereby the effect of the large-scale nonuniformities of the map. Hence by changing the boundary conditions we obtain different variance decay factors for the same straining properties of the map. The rate of variance decay is therefore nonuniversal.

APPENDIX: EVOLUTION OF A GAUSSIAN UNDER STRAIN AND DIFFUSION

In this appendix, we study the evolution of Gaussians under strain and diffusion and derive the parameter evolution in Gaussian description (37) and (38).

A well-known solution of the one-dimensional diffusion equation (12) is a Gaussian with width increasing proportional to $\sqrt{\kappa t}$:

$$\Theta(x,t) = \frac{M}{\sqrt{4\pi\kappa t}} \exp\left(-\frac{x^2}{4\kappa t}\right). \tag{A1}$$

The Gaussian's mean $\int dx\, \Theta$ is in this notation given by its amplitude parameter M. In the following, we use this solution to describe the evolution of any Gaussian,

$$g_{\sigma,A}(x) = A \exp\left(-\frac{x^2}{4\sigma^2}\right), \tag{A2}$$

with amplitude A and width σ under the combined effect of strain and diffusion.

Let us first consider the effect of a strain α. The strain transforms the space coordinate according to $x \to x/\alpha$, the amplitude is not affected by the straining process. The Gaussian's evolution, expressed in parameters A and σ, is then given by

$$A \to A, \tag{A3}$$

$$\sigma \to \alpha\sigma. \tag{A4}$$

Assume now that the Gaussian is subject to diffusion for a time T. We can easily calculate the Gaussian's width and amplitude after the diffusion process by writing it in terms of the solution (A1) of the diffusion equation. If the parameters of the solution are chosen as

$$M = \sqrt{4\pi}\sigma A, \tag{A5}$$

$$t = \frac{\sigma^2}{\kappa}, \tag{A6}$$

the solution has amplitude A and width σ. The Gaussian after the diffusion process is then simply obtained by calculating the solution for $t+T$,

$$\Theta(x,t+T) = \frac{\sqrt{4\pi}\sigma A}{\sqrt{4\pi\kappa\left(\frac{\sigma^2}{\kappa}+T\right)}} \exp\left[-\frac{x^2}{4\kappa\left(\frac{\sigma^2}{\kappa}+T\right)}\right]. \tag{A7}$$

Comparing Eq. (A7) with the initial Gaussian, the diffusion process, expressed in parameters, reads

$$A \to \frac{\sigma}{\sqrt{\sigma^2+\kappa T}}A, \tag{A8}$$

$$\sigma \to \sqrt{\sigma^2+\kappa T}. \tag{A9}$$

Combining the straining process (A5), (A6) with the diffusion process (A8), (A9) yields the evolution of the Gaussians in the Gaussian description (37) and (38).

[1] J. Ottino, *The Kinematics of Mixing: Stretching, Chaos, and Transport* (Cambridge University Press, Cambridge, 1989).

[2] R. Pierrehumbert, Chaos, Solitons Fractals **4**, 1091 (1994).

[3] R. Pierrehumbert, Chaos **10**, 61 (2000).

[4] V. Toussaint, P. Carrière, and F. Raynal, Phys. Fluids **7**, 2587 (1995).

[5] T. Antonsen, Z. Fan, E. Ott, and E. Garcia-Lopez, Phys. Fluids **8**, 3094 (1996).

[6] E. Balkovsky and A. Fouxon, Phys. Rev. E **60**, 4164 (1999).

[7] P. Durbin, J. Fluid Mech. **100**, 279 (1980).

[8] P. Flohr and J. Vassilicos, J. Fluid Mech. **348**, 295 (1997).

[9] A. Wonhas and J. Vassilicos, J. Fluid Mech. **442**, 359 (2001).

[10] D. Fereday, P. Haynes, A. Wonhas, and J.C. Vassilicos, Phys. Rev. E **65**, 035301(R) (2002).

[11] J. Farmer, E. Ott, and J. Yorke, Physica D **7**, 153 (1983).

[12] V. Toussaint and P. Carrière, Int. J. Bifurcation Chaos Appl. Sci. Eng. **9**, 443 (1999).

[13] B.J. Bayley and S. Childress, Geophys. Astrophys. Fluid Dyn. **44**, 211 (1988).

[14] B.J. Bayley and S. Childress, Geophys. Astrophys. Fluid Dyn. **49**, 23 (1989).

[15] S. Childress and A.D. Gilbert, *Stretch, Twist, Fold: The Fast Dynamo*, Lecture Notes in Physics: Monographs, Vol. 354 (Springer-Verlag, Berlin, 1995).

[16] E. Ott and T. Antonsen, Phys. Rev. A **39**, 3660 (1989).

[17] Y. Hu and R. Pierrehumbert, J. Atmos. Sci. **58**, 1493 (2001).

[18] G. Pedrizetti and J. Vassilicos, J. Fluid Mech. **406**, 109 (2000).